Graphene Oxide Immobilized Binuclear Biomimetic Catalyst for Triclosan Degradation in Aqueous Solution

(Pemangkin Biomimetik Binukleus Grafin Oksida Tidak Bergerak kepada Degradasi Triklosan dalam Larutan Akues)

Xue-Fei Zhou[1,2,*] & Shun-Yang Chen[1]

[1]Fujian Provincial Key Laboratory of Marine Ecological Conservation and Restoration, Third Institute of Oceanography, Ministry of Natural Resources, 361005 Xiamen, China
[2]Faculty of Chemical Engineering, Kunming University of Science and Technology, 650500 Kunming, China

ABSTRACT

Biomimetic catalysts, Zn(salen), Zn(Phe-TPP), $ZnPSC_6$ and graphene oxide (GO) immobilized $ZnPSC_6$ ($ZnPSC_6$/GO), were fabricated. These biomimetic catalysts were tested for catalytic *decomposition* of emerging contaminant triclosan (TCS). Catalysts were characterized using Brunauer-Emmett-Teller (BET), X-ray Diffraction (XRD), Fourier Transform infrared (FTIR), and Raman spectra. The reaction processes were studied using HPLC, and the treated solutions were tested based on total carbon content (TCC) analysis and toxicity analysis. The impacts of catalysts on TCS degradation were investigated through testing removal efficiency, total carbon content (TCC) and ecotoxicity. The results showed that $ZnPSC_6$/GO displayed high activity due to salen-porphyrin binuclear active sites and immobilization into GO compared with Zn(salen), Zn(Phe-TPP), and $ZnPSC_6$. Finally, the reaction conditions of TCS oxidation catalyzed by $ZnPSC_6$/GO has been preliminarily discussed. In these conditions, high removal efficiency was observed (96.7%; [$ZnPSC_6$/GO] = 3.0 ppm, [TCS] = 0.02 mmol/L, [H_2O_2] = 0.60 mmol/L, T = 70 °C, t = 90 min, pH = 8).

Keywords: Biomimetic catalysis; degradation; salen-porphyrin complex; TCS

ABSTRAK

Pemangkin biomimetik, Zn(salen), Zn(Phe-TPP), $ZnPSC_6$ dan grafin oksida (GO) tidak bergerak $ZnPSC_6$ ($ZnPSC_6$/GO) telah dihasilkan. Pemangkin biomimetik ini telah diuji untuk penguraian pemangkin bagi triklosan cemaran memuncul (TCS). Pemangkin tersebut telah dicirikan menggunakan Brunauer-Emmett-Teller (BET), pembelauan Sinar-X (XRD), transformasi Fourier inframerah (FTIR) dan spektrum Raman. Proses tindak balas telah dikaji menggunakan HPLC dan larutan yang telah dirawat diuji berdasarkan analisis jumlah kandungan karbon (TCC) dan analisis ketoksikan. Kesan pemangkin pada degradasi TCS telah dikaji melalui ujian kecekapan penyingkiran, jumlah kandungan karbon (TCC) dan ekoketoksikan. Keputusan menunjukkan bahawa $ZnPSC_6$/GO menunjukkan aktiviti yang tinggi disebabkan oleh tapak aktif binukleus salen-porfirin dan imobilisasi ke dalam GO berbanding dengan Zn(salen), Zn(Phe-TPP) dan $ZnPSC_6$. Akhirnya, keadaan tindak balas pengoksidaan TCS yang dimangkinkan oleh $ZnPSC_6$/GO telah dibincangkan terlebih dahulu. Oleh itu, kecekapan penyingkiran tertinggi telah diperhatikan (96.7%; [$ZnPSC_6$/GO] = 3.0 ppm, [TCS] = 0.02 mmol/L, [H2O2] = 0.60 mmol/L, T = 70 °C, t = 90 min, pH = 8).

Kata kunci: Degradasi; pemangkin biomimetik; salen-porfirin kompleks; TCS

INTRODUCTION

In the field of personal care products such as toothpaste, soap, and food packaging, triclosan (TCS, $C_{12}H_7Cl_3O_2$), as a synthetic chlorinated aromatic compound and a typical antibacterial agent, has found an increasingly concern in recent years. Because TCS is chemical potentially toxic compound to the environment and biohealth owing to its properties being lipophilic, accumulative, toxic, and persistent. Further, chlorine as disinfectant in water could react with TCS to form chlorinated triclosan derivatives

(CTDs) and CTDs further transform to polychlorinated dioxin upon the exposure of solar irradiation (Szychowski et al. 2021; Wilburn et al. 2021). Classified as an emerging contaminant, the TCS concentration found in wastewater and surface water are generally in the μg/L and ng/L range. However, in human milk and urine samples, the concentration of TCS is respectively found from 20 to 300 ng/g and of 0.01 to 38 ng/mL (Naidu et al. 2016; Pintado-Herrera et al. 2014). It is thus difficult to degrade this class of contaminants by conventional water treatment processes such as physicochemical and biological processes due to their low concentrations in the environment (Mulla et al. 2020; Savunthari et al. 2021; Wang & Wang 2018; Wang et al. 2021). For this reason, biomimetic complexes may be considered to be used as catalysts as they combine chemo-enzymatic performance (Guo et al. 2021).

Kaur et al. (2019) reported that in removal of triclosan from water, the removal rate of triclosan was different when different activated carbons were employed, suggesting that biomimetic modified activated carbon exhibited the maximum adsorption capacity of 395.2 mg/g in contrast to 71.5 mg/g obtained for unmodified activated carbon. Further, a biomimetic hollow fiber module comprising an active layer of polyamide thin film composite (TFC) with integrated aquaporin proteins was used to reject triclosan, the rejection obtained for triclosan was higher than 93% (Salamanca et al. 2021). In dechlorination of triclosan by using biomimetic or enzymatic systems, it was found that high dechlorination selectivity was only attained by using enzyme, while both selectivity and efficiency were obtained by using biomimetic systems (Souchier et al. 2016). In addition, a study suggested that metal salen complexes were effective catalysts used in triclosan oxidation reactions, however, immobilization of complex into graphene oxide may be effective method for improving removal of triclosan in aqueous solution (Qian et al. 2019). In this study, the catalytic performance can be improved by the condensation reaction of 3,5-dibromosalicylaldehyde with ArGO (aminated reduced graphene oxide) followed by the complexing reaction with copper acetate monohydrate (DArGO-Cu). The mechanism for DArGO-Cu to activate oxidant was the more generation of radicals. Catalytic degradation of triclosan by hydrogen peroxide in the presence of the copper salen Schiff base was evaluated under various conditions. The results showed that TCS was removed by 80.5% within 30 min at optimal reaction conditions. The dominant reactive oxygen species (ROS) involved in the reaction was identified as OH radical. The results suggested that the Schiff base is a promising catalyst for catalyzing oxidative degradation of TCS by H_2O_2 in aqueous solution under neutral condition (Peng et al. 2019). In contrast to metallosalen complex, metalloporphyrin affords high efficiency but low selectivity in degradation of pollutants (Zhao et al. 2019). High efficiency of TCS degradation was obtained (greater than 90%) using metalloporphyrin. The results showed that the immobilized metalloporphyrin has practically the high performance compared to the free form. Activation by metalloporphyrin for triclosan (TCS) degradation was investigated. Concentration of Cl^- showed a dual effect on the TCS degradation. Hydroxyl radicals, superoxide and non-radical single oxygen contributed to the degradation of TCS. Dichlorination, hydroxylation, cyclization, and other bond breaking reaction were inferred as the TCS degradation pathways (Banfi et al. 2006).

Therefore, it is highly desirable that metallosalen complex and metalloporphyrin should be combined, such as binuclear salen-porphyrin complex with two active sites within one complex. The catalytic activity of binuclear complex [Fe(III)(BPMP)Cl(mu-O)Fe(III)Cl^{-3}], as a functional biomimetic analog to methane monooxygenase, was evaluated in cyclohexane oxidation using H_2O_2 as oxidant. Conversions up to 19.2% were observed (12.6 and 6.6% yields for cyclohexanol and cyclohexanone, respectively) (Esmelindro et al. 2005). Both binuclear copper complexes $[\{CuI(L_1)\}_2][OTf]_2$ (1) and $[\{CuII(L_2)Cl\}_2]$ (2) have been shown to be excellent catalysts for the cyclopropanation of various olefins with ethyl diazoacetate (EDA), with catalyst 1 found to be marginally superior to 2 (Das et al. 2012). Porphyrin-salen compound can be obtained by covalently linking by a flexible alkoxy chain (Zhao et al. 2006). Previous studies in our laboratory have shown that the immobilization of Co(salen) on graphene oxide is able to increase the oxidation of lignin (Zhou & Lu 2016); The combination of laccase and Cu(salen) did extend degradation of refractory lignin units (Zhou 2020).

Further, based on the literatures, it is found that no research is conducted on the influence of binuclear salen-porphyrin complex for triclosan degradation. Hence, in this paper, an attempt is made to investigate the influence of the combination of metallosalen complex and metalloporphyrin in the salen-porphyrin complex and the immobilization of salen-porphyrin complex into GO towards triclosan degradation in aqueous solution.

Materials and Methods

Chloroform (Sinopharm Chemical Reagent Co. Ltd., China) was dried with $NaHCO_3$ and $CaCl_2$, and distilled prior to use. Triclosan (TCS > 98%) and graphene oxide (GO, 99.0%) were acquired from Sigma-Aldrich and stored at 4 °C. All other chemicals (Sinopharm Chemical Reagent Co. Ltd., China) were of analytical grade unless specifically noted otherwise. Milli-Q-Plus ultrapure water was used in all experiments.

CATALYSTS FABRICATION

Zn(salen) (Figure 1) was synthesized as follows. Salicylaldehyde (0.02 mol) reacted with ethylenediamine (0.01 mol) in ethanol (75 mL) by refluxing for 2 h. The crude product was purified by washing with petroleum ether and recrystallization in ethanol. Salen ($C_{16}H_{16}N_2O_2$), ^{1}H-NMR (300 MHz, CDCl3, TMS, δ ppm): 13.22 (2H, s, OH), 8.35 (2H, s, CH=N), 7.32-6.80 (8H, m, Ar-H), 3.94 (4H, s, N-CH2CH2-N); FTIR (KBr pellets, cm^{-1}): 3422 (OH), 3053 (C=C), 2925, 2892 (Aliph-H), 2732-2584 (hydrogen bonding), 1637 (C=N), 1602, 1500, 1453 (Ph); Element analysis: $C_{16}H_{16}N_2O_2$; 71.55% C (71.64%), 5.64% H (5.97%), 10.58% N (10.44%), 11.51% O (11.94%). Then, the salen (1.18 g) reacted with zinc acetate (1.1 g) in ethanol (60 mL) by refluxing for 1 h. The crude product was purified by washing with water and recrystallization in chloroform/petroleum ether to obtain Zn(salen). Zn(salen) ($ZnC_{16}H_{14}N_2O_2$), 19.72% Zn (19.63%), 58.27% C (58.00%), 4.15% H (4.22%), 8.38% N (8.45%), 9.62% O (9.66%).
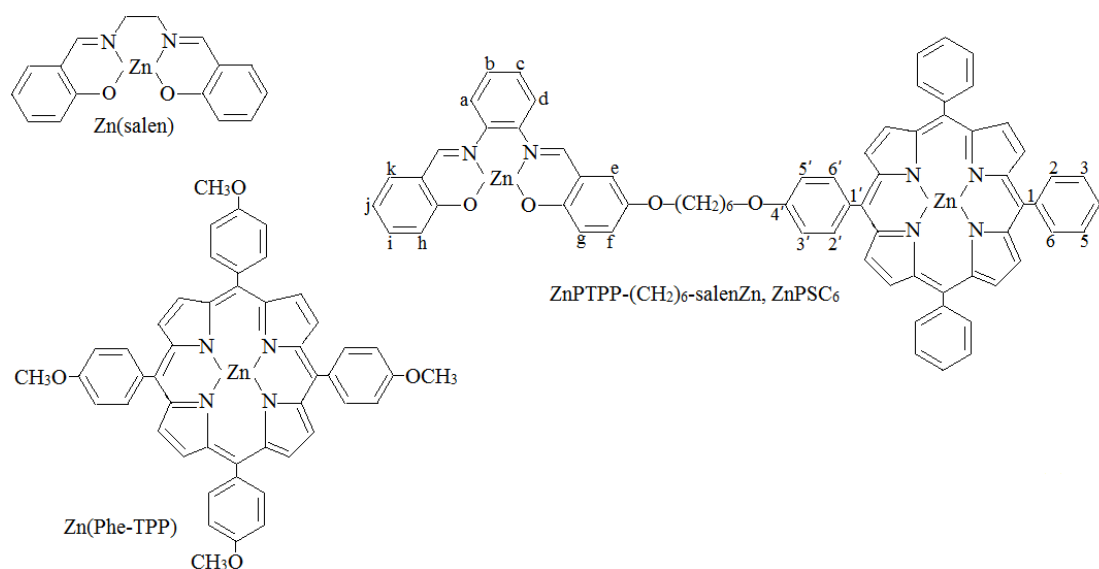

FIGURE 1. Zn(salen), Zn(Phe-TPP) and ZnPSC$_6$

Zn(Phe-TPP) (Figure 1) was synthesized as follows. The first step was to prepare N-chloroacetyl phenylalanine and 5-(p-hydroxylphenyl)-10,15,20- tris(p-chlorophenyl) porphyrin using a method developed by Huang et al. (1983). 5-*p*-(N-Phenylalanine formyl methoxyl) phenyl-10,15,20-tris(p-chlorophenyl) porphyrin (Phe-TPP) was then synthesized *via* reaction of N-chloroacetyl phenylalanine (0.14 mol) and 5-(p-hydroxylphenyl)-10,15,20-tris(p-chlorophenyl) porphyrin (0.40 mol) in DMF (60 mL) in the presence of pyridine (60 mL) and potassium carbonate (2 g) and was purified by a neutral alumina column chromatography. Then, Phe-TPP reacted with zinc acetate (0.2 mmol) by refluxing in DMF for 30 min to obtain Zn(Phe-TPP). The crude product was purified by elution with alumina column chromatography and recrystallization in chloroform-ethanol. Zn(Phe-TPP) ($ZnC_{55}H_{36}O_4N_5Cl_3$), 65.63% C (65.88%), 3.37% H (3.62%), 6.61% N (6.98%). FTIR: -COOH, 1726 cm^{-1}; C-N, 1484 cm^{-1}; porphyrin ring, 1006 cm^{-1}; benzene ring in tetraphenyl porphyrin, 1593/1024/1004/882 cm^{-1}; porphyrin skeleton, 1545/1476/1244/1056 cm^{-1}; zinc porphyrin, 1364 cm^{-1}. ^{1}H-NMR (CDCl$_3$): 8H/Ph-NH$_2$, 5.63; 8H/m-ArH, 6.75-7.47; 8H/O-ArH, 7.60-8.43;

8H/β-pyrrole, 8.96.

ZnPSC$_6$ (Figure 1) was synthesized in nitrogen atmosphere as follows (Zhao et al. 2006). The first step was to prepare 5,10,15-triphenyl-20-p-hydroxyl phenyl porphyrin (HPTPP). *p*-Hydroxyl benzaldehyde (24 g) and benzaldehyde (58 mL) were dissolved in 2000 mL propionic acid and then were transferred to a round bottom flask. The mixture was stirred, heated and refluxed at 140 °C for 20 min. 50 mL Pyrrole was then slowly added to the suspension. The reaction was conducted at 130 °C for 30 min. Then, the reaction mixture was cooled down and left for 12 h at room temperature. Half propionic acid was removed from the reaction mixture by vacuum evaporation, and ethanol was added in equal amount. The reaction was left standing for 24 h to obtain crude HPTPP by filtration. The crude HPTPP was purified by washing with ethanol, elution with chloroform and chloroform/petroleum ether (1:1) in neutral alumina column. The second step was to prepare salen-OH. 620 mg Salicylaldehyde, 550 mg o-phenylenediamine and 700 mg 2,5-dihydroxybenzaldehyde were mixed and stirred in at 30 °C for 20 h. The solution obtained after filtration was evaporated in vacuum and the obtained crude salen-OH was purified by column chromatography and silica gel column. The third step was to prepare salen$(CH_2)_6$Br. 0.25 mmol Salen-OH reacted with 2.5 mmol Br$(CH_2)_6$Br in refluxing in 20 mL acetone in darkness for 5 h in the presence of 3.75 mmol anhydrous potassium carbonate. The mixture was then evaporated in vacuum. The solid was then extracted with chloroform. The salen$(CH_2)_6$Br in organic layers was collected, dried with anhydrous sodium carbonate and purified with chloroform by column chromatography. The fourth step was to prepare HPSC$_6$ (HPTPP-$(CH_2)_6$-salen). 0.30 mmol HPTPP reacted with 3.0 mmol salen$(CH_2)_6$Br in 30 mL acetone in dark at 30 °C for 17 h in the presence of 3.0 mmol anhydrous K$_2$CO$_3$. The mixture was then evaporated in vacuum. The solid was then extracted with chloroform. The crude HPSC$_6$ was obtained in organic phases and purified by elution with chloroform in silica gel column. The fifth step was to prepare ZnPSC$_6$ (ZnPTPP-$(CH_2)_6$-salenZn). 0.30 mmol HPSC$_6$ reacted with zinc acetate in refluxing in chloroform for 5 h. The mixture was then evaporated in vacuum. The crude ZnPSC$_6$ was purified by elution with chloroform in silica gel column. Elemental analysis: ZnPSC$_6$: Zn$_2$C$_{70}$H$_{52}$N$_6$O$_4$, 66.13% C (66.07%), 4.32% H (4.11%), 6.16% N (6.51%); ^{1}H-NMR (CDCl$_3$): $(CH_2)_n$, 1.244-1.651; S-O-CH$_2$, 3.413; P-O-CH$_2$, 4.192; S-phenyl a~d, 6.973-6.976; P-phenyl 4, 7.260-7.296; S-phenyl e~k, 7.392-7.414; P-phenyl 3,5/P-phenyl 3',5', 7.773-7.876; P-phenyl 2,6/P-phenyl 2',6', 8.112-8.202; S-C=N, 8.596/8.604; p-pyrrole-H, 8.93-8.97.

The sixth step was to prepare GO-immobilized ZnPSC$_6$ (ZnPSC$_6$/GO) as described in literature by Cooke and Smith (1994). ZnPSC$_6$ (0.04 g) was fully dispersed in N, N-dimethylformamide (DMF, 20 mL) with the help of ultrasonication. The suspension containing 620 mL water and 16 g GO was then added. The mixture was stirred under ultrasonication at room temperature for 5 h. Then, the mixture was filtered to obtain the solid. The solid was washed with water and vacuum dried at 50 °C. The resulting GO immobilized ZnPSC$_6$ was denoted ZnPSC$_6$/GO. The loading capacity was ~0.6 g/mg, which was based on the zinc analysis (PerkinElmer Optima 8300 ICP-AES). The specific surface area was characterized with Brunauer-Emmett-Teller (BET) equation with a Micromeritics ASAP-2020 (USA). The XRD pattern was recorded with Rigaku Dmax X-ray diffractometer (Ni-filtered, Cu Kα radiation, 40 kV and 30 mA, 2θ, 5-40°, scanning speed 6°/min). FTIR spectra were recorded in the range of 400-4000 cm^{-1} on a Nicolet Impact 410 spectrometer. Raman spectra was obtained at an excitation wavelength laser of 530 nm on confocal micro-Raman spectrometer (Almega XR).

DEGRADATION OF TCS

TCS was degraded in a flask under magnetic stirring at different reaction conditions using hydrogen peroxide as oxidant in the presence of catalyst. At the same time, the pH of the solution was regulated with buffer solution. 2 mL samples were collected from the flask via the syringe at the different reacting time, then filtered and saved for further analysis. The content of TCS was analyzed with HPLC equipped with Zorbax Eclipse Plus C18 column (250 mm × 4.6 mm × 5 μm) using methanol/water mixture (4:1 v/v) as mobile phase. The flow rate of mobile phase was 1.0 mL/min. The total carbon content (TCC) analysis was performed using Vario EL Elemental Analyzer. The toxicity of the solutions was obtained by a Microtox Model 500 Toxicity Analyzer, using a freeze-dried preparation of marine bacterium *Vibrio fischeri* (*Photobacterium phosphoreum*) (Thongrom et al. 2014).

RESULTS AND DISCUSSION

CHARACTERIZATION OF ZnPSC$_6$/GO

The surface areas of GO and ZnPSC$_6$/GO were 627.1 m^2/g and 583.4 m^2/g, respectively. The low surface area of ZnPSC$_6$/GO compared to GO indicated the presence of ZnPSC$_6$/GO within the supercages of GO (Mohamad

et al. 2021).

Figure 2 shows the XRD patterns of GO and ZnPSC$_6$/GO. As shown in Figure 2, due to oxidation of graphite (26.5°, Figure 2(a)), the diffraction peak of GO at 10.8° may be assigned to the reflection of GO (001) plane (Figure 2(b)), demonstrating that some oxygen-containing groups were introduced between the graphite layers (Stobinski et al. 2014). After the immobilization of ZnPSC$_6$ into GO, the diffraction peak of GO at 10.8° was observed but its intensity decreased. This suggested that the immobilization did not destroy the sheet structure of GO. Meanwhile, in XRD analysis, the peaks at 2θ = 22.5° of GO and ZnPSC$_6$/GO indicated the amorphous silicon derived from 3-aminopropyltrimethoxysiloxane after graphene oxidation (Wu et al. 2021).
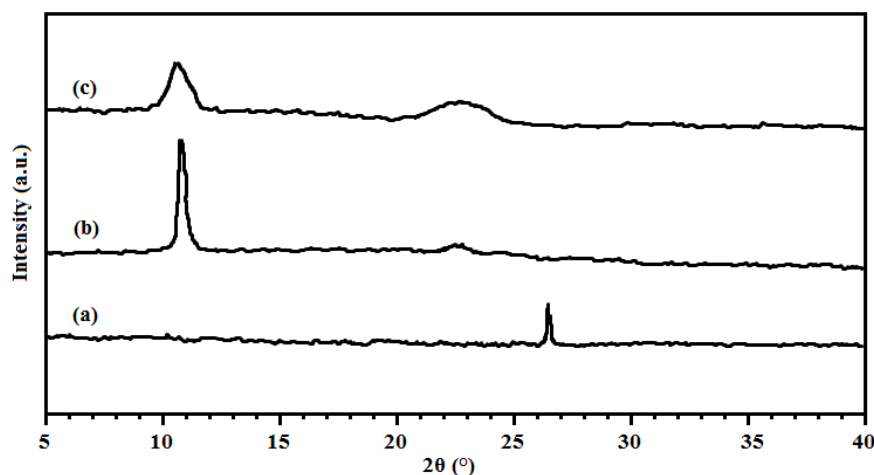

FIGURE 2. XRD spectra of (a) graphene, (b) GO and (c) ZnPSC$_6$/GO

It can be observed by comparing the FTIR spectra of GO and ZnPSC$_6$/GO in Figure 3 that the change occurred after immobilization was applied. The broad peak at 3400 cm^{-1} corresponded to hydroxyl groups in GO. The peaks corresponding to the absorptions at 1724 cm^{-1} and 1626 cm^{-1} were the characteristic peaks of the stretching vibration of C=O and C=C double bond of GO, respectively, and the peaks at 1217 cm^{-1} and 1050 cm^{-1} indicated the C-OH and C-O bonds of GO, respectively. In addition, the FTIR spectra in Figure 3 showed the existence of functional groups on Si-O-Si and Si-O-C, as indicated by the peaks at 1104 cm^{-1} and 1022 cm^{-1}, indicating that ZnPSC$_6$ was linked with GO. As for the existence of ZnPSC$_6$ within GO, additional peaks appeared at wavenumber values of 3052, 2922/2850, 1598, 1486, 1268, 1166, 945, 798/752, 528, and 432 cm^{-1}, corresponding to the salenph C-H, CH$_2$/C-H, salen C=N, pyrrole C=N, Ph ring C-C, Ph ring C-O, Ph ring in C-H, Ph ring out C-H/Ph ring out C-H, Zn-N, and Zn-O, respectively (Al-Musawi et al. 2021; Pfaffeneder-Kmen et al. 2017; Zhao et al. 2006).
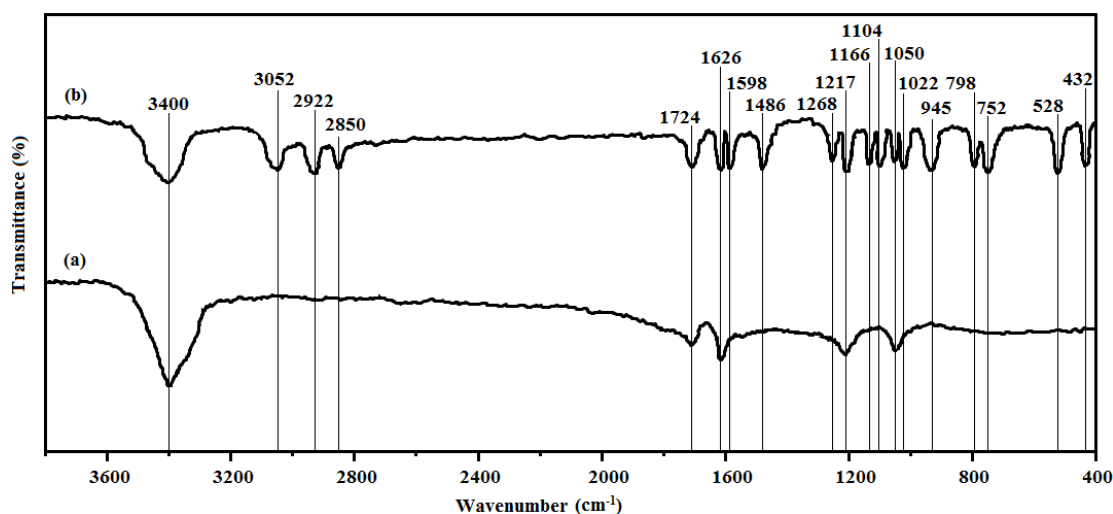

FIGURE 3. FTIR spectra of (a) GO and (b) ZnPSC$_6$/GO

Raman spectroscopy is often used as a principal tool to investigate the ordered and disordered structure of carbon materials such as GO (Abouelsayed et al. 2017). Shown in Figure 4 were the Raman spectra of GO and ZnPSC$_6$/GO. The Raman plots of GO and ZnPSC$_6$/GO showed two distinct bands at about 1332 and ~1600 cm^{-1}, which were the D and G bands, respectively. It was found that compared to the G band of GO at 1597 cm^{-1}, that of ZnPSC$_6$/GO blue shifted to 1610 cm^{-1}, plausibly due to local stress caused by the bond between GO and complex, confirming that oxygen-containing groups of GO were introduced into the ZnPSC$_6$ and confirming that ZnPSC$_6$ was immobilized into GO (Beams et al. 2015).
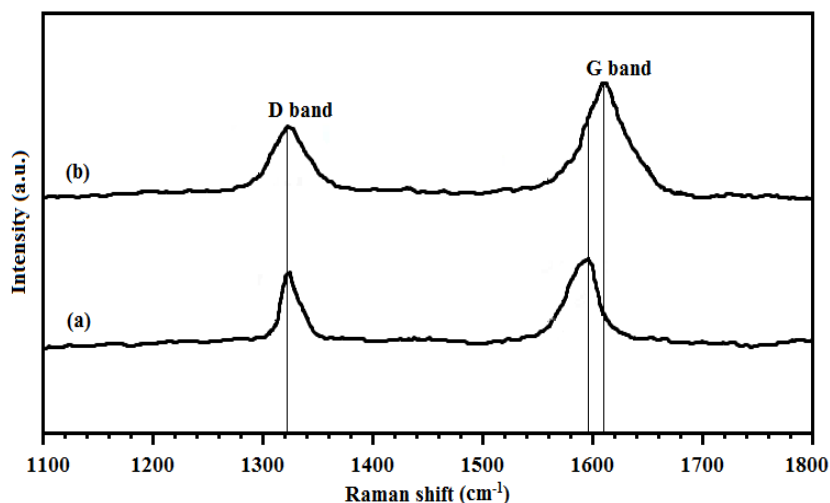

FIGURE 4. Raman spectra of (a) GO and (b) ZnPSC$_6$/GO

DEGRADATION OF TCS

The first step was to evaluate and compare the catalytic activity of different catalysts during catalytic oxidation of TCS. As shown in Figure 5(a), the removal efficiency of TCS was 30.6, 34.8, and 38.5% for Zn(salen)/H$_2$O$_2$, Zn(Phe-TPP)/H$_2$O$_2$, and ZnPSC$_6$/H$_2$O$_2$ systems at 40 °C in 90 min, respectively. The results showed that chemical structure and active sites did contribute to the effect on catalytic activity of complexes. The well-defined structural ZnPSC$_6$ had two active sites of salen and porphyrin to activate H$_2$O$_2$ for TCS degradation, thus improving the removal efficiency of TCS (Gangemi et al. 2019). Moreover, the results showed that after the immobilization of ZnPSC$_6$ into GO, the obtained removal efficiency of TCS increased as a result, which was due to the layer structure of GO affording more voids to provide more accessibilities of the active centre (Gur et al. 2019). Consequently, ZnPSC$_6$/GO gave the highest removal efficiency of TCS of 42.3%. The binuclear complex ZnPSC$_6$ has two active sites of salen and porphyrin and thus has more active sites compared to Zn(salen) and Zn(Phe-TPP) to regulate catalysis by oxo-complex (Li et al. 2018; Maruyama et al. 1991). In addition, ZnPSC$_6$ is a biomimetic complex mimicking an enzyme resulting in high catalytic selectivity (Verma et al. 2021). Further, the porous property of GO make the substrate easily approach active sites of ZnPSC$_6$ (Yunarti et al. 2022). The ecotoxicity and TCC of solutions respectively analyzed by Toxicity Analyzer and Elemental Analyzer were shown in Figure 5(b). Low ecotoxicity was observed for the ZnPSC$_6$/GO treated solution compared with ZnPSC$_6$, Zn(Phe-TPP), Zn(salen), indicating that TCS was deeply mineralized with ZnPSC$_6$/GO because TCC conversion of ZnPSC$_6$/GO treated solution was highest (Samarghandi et al. 2021).

pH of medium was considered as potential effect in the degradation reaction of organic pollutants by catalysis (Elsayed et al. 2020). A batch of experiments, in which the initial pH was set at 5, 6, 7, 8, 9, and 11, was performed to investigate the pH effect on TCS removal. As shown in Figure 6(a), the TCS removal efficiency was highest at pH 8, and low under acidic conditions. Thus, the optimum degradation of TCS by ZnPSC$_6$/GO can be obtained in weak alkali medium. Therefore, weak alkali medium was beneficial to improve the catalytic activity of ZnPSC$_6$ (Meininger et al. 2017; Vargas et al. 2004). Figure 6(b) demonstrated the temperature effect on the oxidation of TCS. When the reaction temperature increased from 20 to
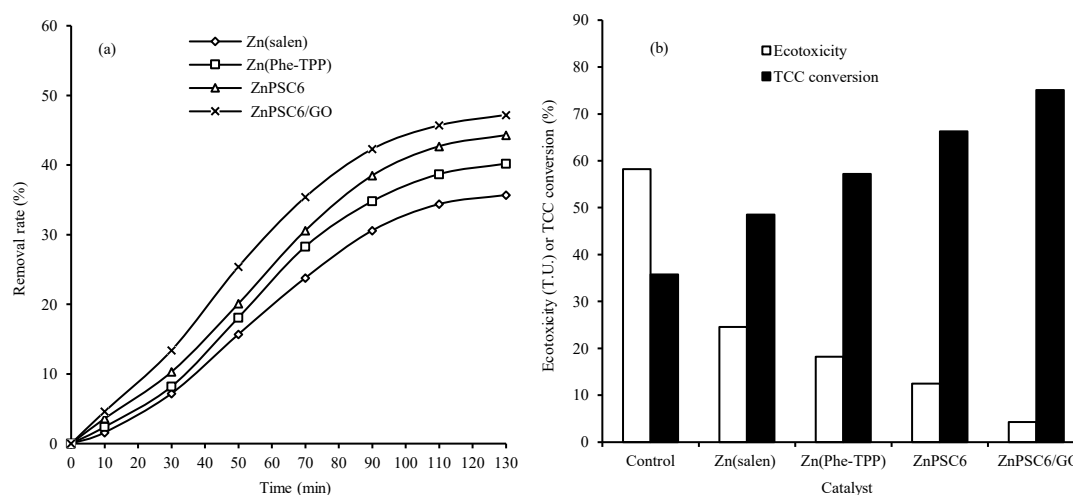
FIGURE 5. Performance comparison of different catalysts during catalytic oxidation of TCS. [TCS] = 0.02 mmol/L, [catalyst] = 2.0 ppm, pH = 7.0, [H_2O_2] = 0.20 mmol/L, T = 40 °C
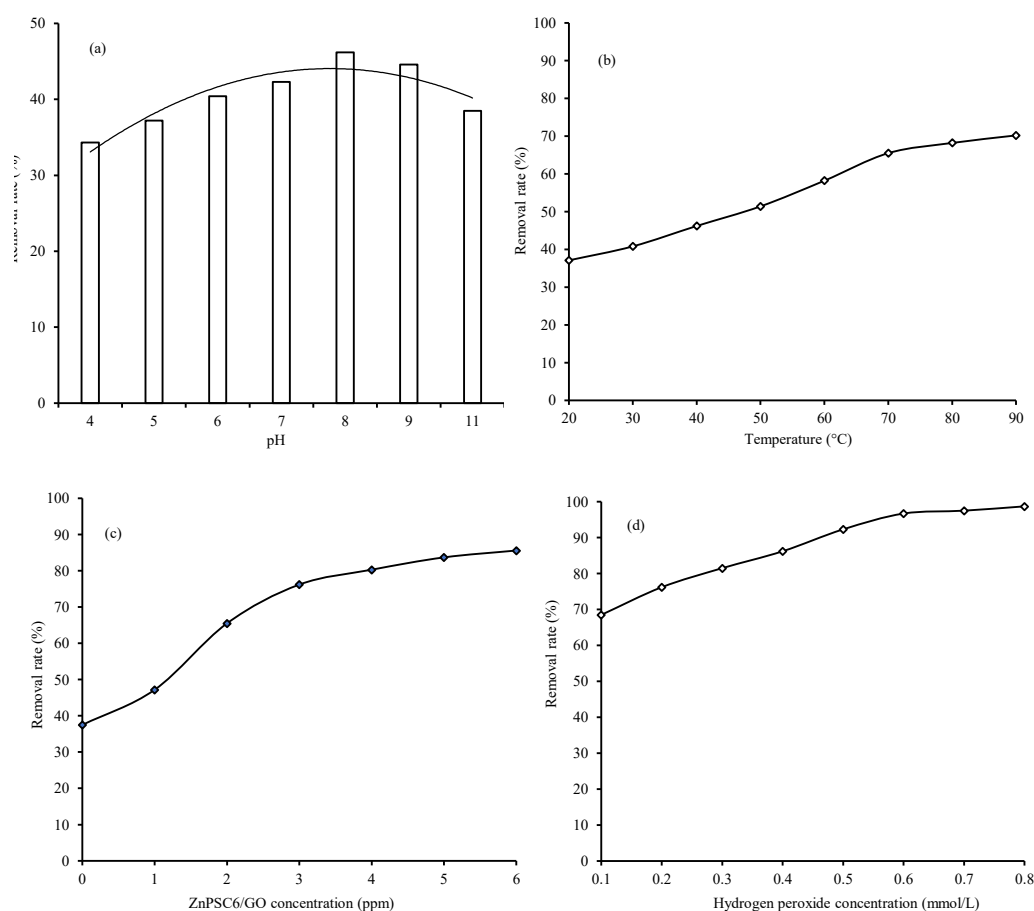

FIGURE 6. Catalytic oxidation of TCS by ZnPSC$_6$/GO. (a) pH effect. [TCS] = 0.02 mmol/L, [ZnPSC$_6$/GO] = 2.0 ppm, [H_2O_2] = 0.2 mmol/L, T = 40 °C, t = 90 min; (b) Temperature effect. [TCS] = 0.02 mmol/L, [ZnPSC$_6$/GO] = 2.0 ppm, [H_2O_2] = 0.2 mmol/L, t = 90 min, pH = 8; (c) ZnPSC$_6$/GO concentration effect. [TCS] = 0.02 mmol/L, [H_2O_2] = 0.2 mmol/L, T = 70 °C, t = 90 min, pH = 8; (d) Hydrogen peroxide concentration concentration effect. [ZnPSC$_6$/GO] = 3.0 ppm, [TCS] = 0.02 mmol/L, T = 70 °C, t = 90 min, pH = 8

70 °C, the removal of TCS increased from 37.1 to 65.5%. Further increase of reaction temperature had little effect on TCS degradation. $ZnPSC_6$/GO concentration effect was also discussed in the degradation of TCS. The reaction afforded increasing removal of TCS with increasing $ZnPSC_6$/GO concentration (Figure 6(c)). This may be explained that increasing $ZnPSC_6$/GO concentration resulted in increasing catalytic sites to activate H_2O_2 (Huang et al. 2021). When hydrogen peroxide was used as oxygen source, the H_2O_2 concentration exhibited positive effect on TCS degradation (Crincoli & Huling 2021). It can be seen from Figure 6(d) that when H_2O_2 concentration increased from 0.1 to 0.6 mmol/L, the removal of TCS gradually increased from 68.5 to 96.7% and remained little chang with further increase of H_2O_2. Thus, the optimum H_2O_2 concentration was 0.6 mmol/L.

CONCLUSION

In this work, a biomimetic complex based catalyst structure, $ZnPSC_6$, with binuclear salen-porphyrin active sites, and in the form of immobilization into GO ($ZnPSC_6$/GO), was fabricated and used to activate H_2O_2 to degrade TCS in water. The characterization of catalysts indicated that $ZnPSC_6$ and GO were combined in immobilized catalyst, which produced high activity than $ZnPSC_6$, Zn(Phe-TPP) and Zn(salen). Attributed to the improvement of performance from immobilization of $ZnPSC_6$ into GO and the synergic effect of $ZnPSC_6$ and GO, the $ZnPSC_6$/GO showed excellent performance in H_2O_2 activation for degrading TCS. Compared with other biomimetic catalysts such as Zn(salen), Zn(Phe-TPP), $ZnPSC_6$, the $ZnPSC_6$/GO exhibited distinct advantage over activation for the outstanding degradation efficiency of TCS. In addition, removal efficiency of 96.7% was obtained under the optimum reaction conditions.

ACKNOWLEDGEMENTS

REFERENCES

Abouelsayed, A., Anis, B., Hassaballa, S., Khalil, A.S.G., Rashed, U.M., Eid, K.A., Al-Ashkar, E. & El Hotaby, W. 2017. Preparation, characterization, Raman, and Terahertz spectroscopy study on carbon nanotubes, graphene nano-sheets, and onion like carbon materials. *Materials Chemistry and Physics* 189: 127-135.

Al-Musawi, T.J., Rajiv, P., Mengelizadeh, N., Mohammed, I.A. & Balarak, D. 2021. Development of sonophotocatalytic process for degradation of acid orange 7 dye by using titanium dioxide nanoparticles/graphene oxide nanocomposite as a catalyst. *Journal of Environmental Management* 292: 112777.

Banfi, S., Caruso, E., Buccafurni, L., Battini, V., Zazzaron, S., Barbieri, P. & Orlandi, V. 2006. Antibacterial activity of tetraaryl-porphyrin photosensitizers: An *in vitro* study on Gram negative and Gram positive bacteria. *Journal of Photochemistry and Photobiology B: Biology* 85(1): 28-38.

Beam, R., Cancado, L.G. & Novotny, L. 2015. Raman characterization of defects and dopants in graphene. *Journal of Physics-Condensed Matter* 27(8): 083002.

Cooke, P.R. & Smith, J.R.L. 1994. Alkene epoxidation catalysed by iron(III) and manganese(III) tetraarylporphyrins coordinatively bound to polymer and silica supports. *Journal of the Chemical Society-Perkin Transactions* 1(14): 1913-1923.

Crincoli, K.R. & Huling, S.G. 2021. Contrasting hydrogen peroxide- and persulfate-driven oxidation systems: Impact of radical scavenging on treatment efficiency and cost. *Chemical Engineering Journal* 404: 126404.

Das, R.K., Sarkar, M., Rahaman, S.M.W., Doucet, H. & Bera, J.K. 2012. Binuclear copper complexes and their catalytic evaluation. *European Journal of Inorganic Chemistry* 2012(10): 1680-1687.

Esmelindro, M.C., Oestreicher, E.G., Marquez-Alvarez, H., Dariva, C., Egues, S.M.S., Fernandes, C., Bortoluzzi, A.J., Drago, V. & Antunes, O.A.C. 2005. Catalytic oxidation of cyclohexane by a binuclear Fe(III) complex biomimetic to methane monooxygenase. *Journal of Inorganic Biochemistry* 99(10): 2054-2061.

Gangemi et al. 2019

Guo, M., Lee, Y.M., Fukuzumi, S. & Nam, W. 2021. Biomimetic metal-oxidant adducts as active oxidants in oxidation reactions. *Coordination Chemistry Reviews* 435: 213807.

Gur, B., Ayhan, M.E., Turkhan, A., Gur, F. & Kaya, E.D. 2019. A facile immobilization of polyphenol oxidase enzyme on graphene oxide and reduced graphene oxide thin films: An insight into *in-vitro* activity measurements and characterization. *Colloids and Surfaces A: Physicochemical and Engineering Aspects* 562: 179-185.

Huang, Z.Y., Wu, P.X., Liu, C.H., Chen, M.Q., Yang, S.S., Dang, Z. & Zhu, N.W. 2021. Multiple catalytic reaction sites induced non-radical/radical pathway with graphene layers encapsulated Fe-N-C toward highly efficient peroxymonosulfate (PMS) activation. *Chemical Engineering Journal* 413: 127507.

Huang, S., Sun, L. & Ye, C. 1983. Studies on the porphyrin compounds. *Chemical Journal of Chinese Universities* 4(3): 381-384.

Kaur, H., Hippargi, G., Pophali, G.R. & Bansiwal, A. 2019. Biomimetic lipophilic activated carbon for enhanced removal of triclosan from water. *Journal of Colloid and Interface Science* 535: 111-121.

Li, J., Fan, Y., Ren, Y., Liao, J., Qi, C. & Jiang, H. 2018. Development of isostructural porphyrinsalen chiral metal-organic frameworks through postsynthetic metalation based on single-crystal to single-crystal transformation. *Inorganic Chemistry* 57(3): 1203-1212.

Maruyama, K., Kobayashi, F. & Osuka, A. 1991. Synthesis and characterization of directly linked salen–porphyrin system with constrained geometries. *Bulletin of the Chemical Society of Japan* 64(1): 29-34.

Meininger, D.J., Arman, H.D. & Tonzetich, Z.J. 2017. Synthesis, characterization, and binding affinity of hydrosulfide complexes of synthetic iron(II) porphyrinates. *Journal of Inorganic Biochemistry* 42: 149-167.

Mohamad, S., Bakhshaei, S., Abdul, M.N.S., Parmin, N.A. & Mahmad, R.S.K. 2021. Free fatty acid from waste palm oil functionalized magnetic nanoparticles immobilized on surface graphene oxide as a new adsorbent for simultaneously detecting hazardous polycyclic aromatic hydrocarbons and phthalate esters in food extracts. *Journal of Nanoscience and Nanotechnology* 21(11)**:** 5522-5534.

Mulla, S.I., Asefi, B., Bharagava, R.N., Saratale, G.D., Li, J.W., Huang, C.L. & Yu, C.P. 2020. Processes for the removal of triclosan in the environment and engineered systems: A review. *Environmental Reviews* 28(1): 55-66.

Naidu, R., Espana, V.A.A., Liu, Y. & Jit, J. 2016. Emerging contaminants in the environment: Risk-based analysis for better management. *Chemosphere* 154: 350-357.

Peng, J., Zhang, Y., Zhang, Y., Chen, M., Zhang, H., Li, J., Liu, H. & Gao, S. 2019. Oxidative removal of triclosan with hydrogen peroxide catalyzed by a schiff base Cu(II)-complex. *Environmental Chemistry* 38: 977-984.

Pfaffeneder-Kmen, M., Casas, I.F., Naghilou, A., Trettenhahn, G. & Kautek, W. 2017. A multivariate curve resolution evaluation of an *in-situ* ATR-FTIR spectroscopy investigation of the electrochemical reduction of graphene oxide. *Electrochimica Acta* 255**:** 160-167.

Pintado-Herrera, M.G., González-Mazo, E. & Lara-Martín, P.A. 2014. Determining the distribution of triclosan and methyl triclosan in estaurine settings. *Chemosphere* 95: 478-485.

Qian, L., Liu, P., Shao, S., Wang, M.J., Zhan, X. & Gao, S.X. 2019. An efficient graphene supported copper salen catalyst for the activation of persulfate to remove chlorophenols in aqueous solution. *Chemical Engineering Journal* 360**:** 54-63.

Samarghandi, M.R., Dargahi, A., Rahmani, A., Shabanloo, A., Ansari, A. & Nematollahi, D. 2021. Application of a fluidized three-dimensional electrochemical reactor with Ti/SnO2-Sb/beta-PbO2 anode and granular activated carbon particles for degradation and mineralization of 2,4-dichlorophenol: Process optimization and degradation pathway. *Chemosphere* 279: 130640**.**

Salamanca, M., López-Serna, R., Palacio, L., Hernández, A., Prádanos, P. & Peña, M. 2021. Study of the rejection of contaminants of emerging concern by a biomimetic aquaporin hollow fiber forward osmosis membrane. *Journal of Water Process Engineering* 40: 101914.

Savunthari, K.V., Arunagiri, D., Shanmugam, S., Ganesan, S., Arasu, M.V., Al-Dhabi, N.A., Chi, N.T.L. & Ponnusamy, V.K. 2021. Green synthesis of lignin nanorods/g-C3N4 nanocomposite materials for efficient photocatalytic degradation of triclosan in environmental water. *Chemosphere* 272: 129801.

Souchier, M., Casellas, C., Ingrand, V. & Chiron, S. 2016. Insights into reductive dechlorination of triclocarban in river sediments: Field measurements and *in vitro* mechanism investigations. *Chemosphere* 144**:** 425-432.

Stobinski, L., Lesiak, B., Malolepszy, A., Mazurkiewicz, M., Mierzwa, B., Zemek, J., Jiricek, P. & Bieloshapka, I. 2014. Graphene oxide and reduced graphene oxide studied by the XRD, TEM and electron spectroscopy methods. *Journal of Electron Spectroscopy and Related Phenomena* 195**:** 145-154.

Szychowski, K.A., Skóra, B. & Wójtowicz, A.K. 2021. Triclosan affects the expression of nitric oxide synthases (NOSs), peroxisome proliferator-activated receptor gamma (PPARγ), and nuclear factor kappa-light-chain-enhancer of activated B cells (NF-κB) in mouse neocortical neurons *in vitro. Toxicology in Vitro* 73: 105143.

Thongrom, B., Amornpitoksuk, P., Suwanboon, S. & Baltrusaitis, J. 2014. Photocatalytic degradation of dye by Ag/ZnO prepared by reduction of Tollen's reagent and the ecotoxicity of degraded products. *Korean Journal of Chemical Engineering* 31: 587-592.

Vargas, G., Hernandez, I., Hopfl, H., Ochoa, M.E., Castillo, D., Farfan, N., Santillan, R. & Gomez, E. 2004. Preparation and structural characterization of three types of homo- and heterotrinuclear boron complexes: Salen{[B-O-B][O$_2$BOH]}, salen{[B-O-B][O$_2$BPh]}, and salen{[B-O-B][O$_2$P(O)Ph]}. *Inorganic Chemistry* 43(26)**:** 8490-8500.

Verma, M., Bhaduri, G.A., Kumar, V.S.P. & Deshpande, P.A. 2021. Biomimetic catalysis of CO$_2$ hydration: A materials perspective. *Industrial & Engineering Chemistry Research* 60(13): 4777-4793.

Wang, W., Nadagouda, M.N. & Mukhopadhyay, S.M. 2021. Flexible reusable hierarchical hybrid catalyst for rapid and complete degradation of triclosan in water. *Science of the Total Environment* 766: 144109.

Wang, S.Z. & Wang, J.L. 2018. Degradation of triclosan and its main intermediates during the combined irradiation and biological treatment. *Environmental Technology* 39(9)**:** 1115-1122.

Wilburn, W.J., Jamal, S., Ismail, F., Brooks, D. & Whalen, M. 2021. Evaluation of triclosan exposures on secretion of pro-inflammatory cytokines from human immune cells. *Environmental Toxicology and Pharmacology* 83: 103599.

Wu, S.S., Lan, D.H., Tan, N.Y., Wang, R., Au, C.T. & Yi, B. 2021. Manganese Schiff base immobilized on graphene oxide complex and its catalysis for epoxidation of styrene. *Journal of the Chemical Society of Pakistan* 43(1)**:** 57-66.

1774

Yunarti, R.T., Safitri, T.N., Dimonti, L.C.C., Aulia, G., Khalil, M. & Ridwan, M. 2022. Facile synthesis of composite between titania nanoparticles with highly exposed (001) facet and coconut shell-derived graphene oxide for photodegradation of methylene blue. *Journal of Physics and Chemistry of Solids* 160: 110357.

Zhao, X., Zhang, P., Zhao, Y., Zhang, W., Meng, L., Hou, H., Liu, B., Yang, J. & Hu, J. 2019. The degradation of pollutants catalyzed by metalloporphyrin derivatives. *Environmental Chemistry* 38(9): 2067-2080.

Zhao, X.J., Ruan, W.J., Zhang, Y.H., Dai, F., Liu, D., Zhu, Z.A. & Fan, S.D. 2006. Molecular recognition of porphyrin-salen compound towards N-heterocyclic-guests. *Chinese Journal of Chemistry* 24(8): 1031-1036.

Zhao, X.J., Ruan, W.J. & Zhu, Z.A. 2006. Study on synthesis and spectral properties of porphyrin-salen compounds. *Chinese Journal of Organic Chemistry* 26(8): 1087-1092.

Zhou, X.F. 2020. A one-pot catalysis combining laccase with Cu(salen) for selective removal of refractory lignin units during oxygen delignification of bamboo kraft pulp. *Scientia Forestalis* 127: 39.

Zhou, X.F. & Lu, X. 2016. Co(salen) supported on graphene oxide for oxidation of lignin. *Journal of Applied Polymer Science* 133(44): 44133.

*Corresponding author; email: lgdx602@sina.com